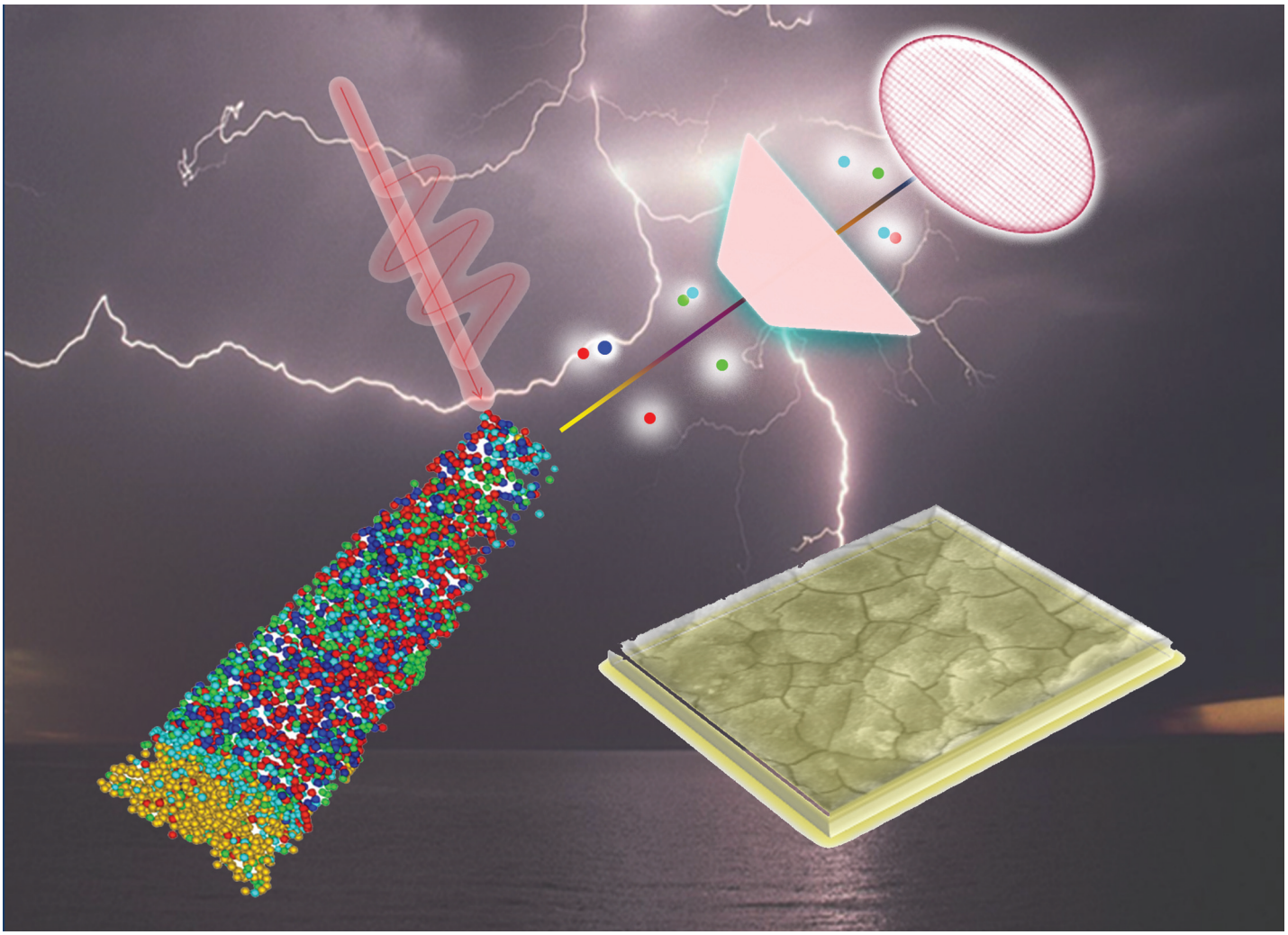

Showcasing research from the Department of Materials Science and Engineering, Tel-Aviv University, Israel & Northwestern University Center for Atom-Probe Tomography, Evanston, IL, USA.

Atomically resolved calcium phosphate coating on a gold substrate

Hydroxyapatite (HAp) coatings have been applied on implants. Electrodeposited coatings have been claimed to entail a precursor phase, similar to biomineralization. Yet, the chemical composition of the initial layer and its thickness have been arguable. Here, atom-probe tomography is utilized for the first time to study such coatings. Its correlative use with transmission electron microscopy provides unprecedented sensitivity that permits the unambiguous identification of a mixture of ACP, DCPD and OCP, tens of nanometers thick, at the heterophase interface. These phases could all eventually transform into HAp.

As featured in:

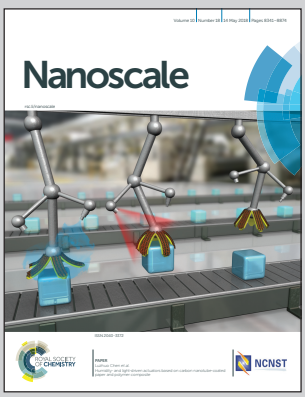

See David N. Seidman, Noam Eliaz *et al.*, *Nanoscale*, 2018, **10**, 8451.

ROYAL SOCIETY OF CHEMISTRY

rsc.li/nanoscale

Registered charity number: 207890

Nanoscale

PAPER

View Article Online
View Journal | View Issue

Cite this: *Nanoscale*, 2018, **10**, 8451

Atomically resolved calcium phosphate coating on a gold substrate†

Noah Metoki,[a] Sung-Il Baik,[b,c] Dieter Isheim,[b,c] Daniel Mandler,[d] David N. Seidman*[b,c,e] and Noam Eliaz*[a]

Received 14th January 2018,
Accepted 7th March 2018

DOI: 10.1039/c8nr00372f

rsc.li/nanoscale

Some articles have revealed that the electrodeposition of calcium phosphate (CaP) coatings entails a precursor phase, similarly to biomineralization *in vivo*. The chemical composition of the initial layer and its thickness are, however, still arguable, to the best of our knowledge. Moreover, while CaP and electrodeposition of metal coatings have been studied utilizing atom-probe tomography (APT), the electrodeposition of CaP ceramics has not been heretofore studied. Herein, we present an investigation of the CaP deposition on a gold substrate. Using APT and transmission electron microscopy (TEM) it is found that a mixture of phases, which could serve as transient precursor phases to hydroxyapatite (HAp), can be detected. The thickness of these phases is tens of nanometers, and they consist of amorphous CaP (ACP), dibasic calcium phosphate dihydrate (DCPD), and octacalcium phosphate (OCP). This demonstrates the value of using atomic-resolved characterization techniques for identifying the precursor phases. It also indicates that the kinetics of their transformation into the more stable HAp is not too fast to enable their observation. The coating gradually displays higher Ca/P atomic ratios, a porous nature, and concomitantly a change in its density.

1. Introduction

In the past 30 years, since approval by the U.S. Food and Drug Administration (FDA), calcium phosphate (CaP) coated orthopaedic and dental implants have become very common.[1] The most important CaP for biomedical applications is hydroxyapatite (HAp, $Ca_{10}(PO_4)_6(OH)_2$). The most widely utilized process for the application of CaP coatings on implants is plasma spraying,[1] although in recent years electrochemical deposition (ED) has gained great interest.[2–23]

The nucleation and growth processes of ED CaP coatings have been studied by different research groups, using different substrates and deposition conditions.[5,9,24,25] For example, Eliaz *et al.* investigated the nucleation of CaP on titanium from a dilute solution.[5] They concluded that the ED of CaP involves two stages: (1) instantaneous nucleation, 2-D growth; followed by (2) progressive nucleation, 3-D growth. No discussion of the possible character of a precursor phase was, however, made.

While the structure of bone is reasonably well defined, the process of the bone mineral formation remains controversial. Mineralization *via* transient precursor phases such as amorphous calcium phosphate (ACP), octacalcium phosphate (OCP, $Ca_8(HPO_4)_2(PO_4)_4{\cdot}5H_2O$), and even dibasic calcium phosphate dihydrate (DCPD, brushite, $CaHPO_4{\cdot}2H_2O$) has been suggested.[1,26–30] The similarity between the structures of OCP and HAp has been proposed as providing geometrically favourable conditions for phase transformation from OCP to HAp.[26]

Eliaz *et al.* reported several findings, which may support the presence of a precursor phase (most likely OCP, although ACP was not excluded) during the process of electrocrystallization of HAp.[6–8] Real-time, *in situ* electrochemical quartz crystal microbalance (EQCM) measurements revealed two phenomena during the first 11 min of deposition: (1) an incubation time required for the local pH to increase; and (2) the formation of a precursor phase with a lower mass density and higher charge density. Advanced X-ray photoelectron spectroscopy (XPS) enabled the unambiguous determination of the presence of OCP.[8] Importantly, after implanting rods electrodeposited with CaP coatings in canine trabecular bones of dogs, Eliaz *et al.*[4]

[a]*Biomaterials and Corrosion Lab, Department of Materials Science and Engineering, Tel-Aviv University, Ramat Aviv 6997801, Israel. E-mail: neliaz@tau.ac.il*
[b]*Department of Materials Science and Engineering, Northwestern University, 2220 Campus Drive, Evanston, Illinois 60208-3108, USA. E-mail: d-seidman@northwestern.edu*
[c]*Northwestern University Center for Atom-Probe Tomography (NUCAPT), 2220 Campus Drive, Evanston, Illinois 60208-3108, USA*
[d]*Institute of Chemistry, The Hebrew University of Jerusalem, Edmond J. Safra Campus, Givat Ram, Jerusalem 9190401, Israel*
[e]*NanoAl LLC, Illinois Science+Technology Park, 8025 Lamon Ave, Suite 446, Skokie, IL 60077, USA*

†Electronic supplementary information (ESI) available: Additional information on FIB & SEM. See DOI: 10.1039/c8nr00372f

also found that during early stage mineralization (≤7 d), the Ca/P ratio in the mineralized tissue adjacent to the electrodeposited HAp coating resembles that in OCP, although DCPD or ACP could not be excluded.

Although the presence of a precursor phase being initially electrodeposited was suggested by Eliaz *et al.*,[6–9] the nature of the precursor phase was not studied in detail. In most studies by other groups involving ED, the ED actually creates a metastable phase, such as brushite, which after a post-treatment transforms in an alkaline environment into the more thermodynamically favourable HAp.[31] Our group has recently studied the first steps of ED on gold substrates.[18] The available techniques could not, however, determine the chemistry on a sub-nanometer to nanometer length scale within the material being created, and therefore could not reveal the nature of the initial phase being deposited on the surface of the electrode.

Atom-probe tomography (APT) is a powerful analytical technique for determining the chemistry on a sub-nanometer to nanometer length scale. It offers 3-D imaging and chemical composition measurements at the atomic scale (0.1–0.3 nm spatial resolution in depth, 0.3–0.5 nm laterally).[32–34] This capability has led to the study of a wide range of materials on the sub-nanometer to nanometer length scale for a broad range of physical problems; for example, studies of alloys and superalloys,[35,36] nanowires,[37] nanoparticles,[38] transistors,[39] powders,[40] and even metallic thin films and electrodeposits.[41–44]

APT has also been utilized for studying biomineralization. For example, Gordon *et al.* demonstrated that APT is well-suited for distinguishing between geological fluorapatite and synthetic single crystals of fluorapatite, chlorapatite and HAp, based on their spectrometric fingerprint.[45] This fingerprint and the formation of molecular ions during field evaporation are explained based on the chemistry of the apatite channel ion. Using the synthetic apatites as references, dentin and cortical bone were analyzed as examples of structurally and chemically complex biological nanocomposites. Finally, APT was shown to capture the fibrous nature of the collagenous organic matrix in dentin and to aid in characterizing interfaces. Gordon and Joester utilized APT to reveal 3-D chemical maps of organic fibers in the surrounding nano-crystalline magnetite (Fe_3O_4) mineral in chiton teeth.[46] In another study, Karlsson *et al.* studied bone integration on titanium dental implants and found high concentrations of calcium on the titanium implant after four weeks of healing.[47]

While the fields of CaP and ED of metal coatings have been studied, to the best of our knowledge, the ED of CaP ceramics has heretofore not been analyzed by APT. Since ED CaP is already clinically applied on orthopaedic and dental implants, the study of CaP coatings by APT can provide invaluable information on the initial processes; for example, nucleation, precursor phases and adhesion between the ED coating and the implant surface. Such studies may contribute to a better understanding of the more complex processes of biomineralization *in vivo*.

2. Experimental

2.1 Specimen preparation

Uncoated atom-probe tomographic specimens were first prepared by electropolishing gold wires, using a custom-made electropolishing tool and following a procedure similar to that described by Stoffers *et al.*[48] Briefly, ~15 mm long pieces of gold wire (0.2 mm in diameter) were cut and attached to a copper stub, which was affixed to a manual *xyz* positioning stage. A platinum ring electrode surrounded the nanotip in a cuvette cell containing 3 mL of 50 : 50 HCl : ethanol. A DC power supply was used to apply pulsed voltages varying between 2 and 8 V at room temperature, thus creating a sharp nanotip by means of local necking of the gold wire. The nanotips were further sharpened using dual-beam focused ion-beam (FIB, Helios Nanolab, FEI Co.) microscopy. Electrodeposition was performed in a three-electrode cell containing the sharpened gold wire as a working electrode (cathode), a platinum mesh as a counter electrode, and a Ag/AgCl (1 M KCl) electrode as a reference electrode. The electrolyte solution consisted of 0.61 mM $Ca(NO_3)_2$ and 0.36 mM $NH_4H_2PO_4$ at pH 7.4 (non-buffered) and 37 °C. Electrodeposition was performed at −1.4 V for 1 minute.

2.2 APT analyses

The process of sample preparation by dual-beam FIB for APT characterization is displayed in Fig. S1 (ESI†). Nanotip specimens were then dissected atom-by-atom and atomic plane-by-plane utilizing a LEAP tomograph (LEAP4000X-Si, Cameca, Madison, WI, USA) at the Northwestern University Center for Atom-Probe Tomography (NUCAPT) to measure the chemical compositions of APT nanotip samples. Picosecond pulses of ultraviolet laser light (wavelength ~355 nm) were applied to evaporate individual atoms from APT nanotips at a pulse repetition rate of 200 kHz, a laser energy of 150 pJ per pulse, an average detection rate of 0.01 ions per pulse, and a nanotip temperature of 40 K. The nanotips were maintained at a positive potential, while the evaporation of ions was triggered by the picosecond UV laser pulses. The chemical composition of the electrodeposited CaP on Au was measured by time-of-flight (TOF) mass-to-charge-state ratio spectra. The detection efficiency of the multichannel plate (MCP) detector is 50–60%, and is the same for all elements. Data analyses were performed on the 3-D reconstructions of specimens, utilizing the program IVAS 3.6.8 (Cameca). Each mass spectrum of possible ions was examined carefully, taking into consideration the bath composition and previous publications in the field.

2.3 Transmission electron microscopy (TEM)

Evaporated gold samples were electrodeposited with CaP for 2 h. The samples were then placed in the dual-beam FIB microscope, for lift-out. The CaP layer was covered by an ~200 nm thick platinum overlayer to protect the top surface. A $20 \times 5\ \mu m^2$ sample was ion-milled out and transferred to the Cu grid, utilizing an Omniprobe. The sample was thinned using a dual-beam FIB microscope, employing Ga^+ ion-sputter-

ing, utilizing a final energy of 2 kV at 24 pA (sample preparation is described in ESI Fig. S2†). A JEOL 2100F microscope operating at 200 kV and CrystalMaker™ software package for indexing of SAED patterns were used.[49]

3. Results and discussion

To investigate the atomic contents of the electrodeposited CaP coating and the first phase forming at the heterophase interface, elemental distributions of the coating's heterophase interface with the gold substrate were determined by APT. Fig. 1(a) displays a 3-D local-electrode atom-probe (LEAP) tomographic reconstruction of the field-evaporated atoms (312 000 ions): calcium, phosphorus, oxygen, carbon, hydrogen, and gold atoms. The heterophase interface between the gold substrate and the CaP coating is well defined. The distribution of the five elements in the CaP coating is not completely uniform. The low-density regions (left side, 0–20 nm in the *z*-direction) in the 3-D LEAP tomographic reconstruction may be related to the inherently porous structure of the CaP electrodeposit. This is also supported by TEM images, as shown in Fig. 3(a).

The chemical composition of the CaP coating throughout the first 50 nm of deposition on gold is determined by drawing a line profile along the *z*-direction of the nanotip, that is, its long axis. It is important to note that the length scale of 20–30 nm is comparable to that of the grain size in the ED CaP. We find that while the average Ca/P atomic ratio equals 0.93 in the first 22 nm closest to the Au substrate, it increases to 1.58 within the next 30 nm. This may be related to a bottom layer richer in DCPD and an upper layer richer in OCP and ACP, for example (see their chemical formulae). It is also evident that no major contaminants are present in the coating, besides a small concentration of carbon. The latter is highest at the coating/substrate interface (~7 at%), and decreases to ~2 at% towards the top (outer) side of the coating, see Fig. 1(b). This indicates that the origin of the carbonate is either the electropolishing of the gold substrate or the ED of CaP, and is not common surface impurity (adsorption) from the atmosphere. Carbonate is known as one of the impurities incorporated into biominerals, such as CaP. A CO_3-for-PO_4 substitution has been claimed for apatites prepared in aqueous media.[50]

It has been demonstrated that the stoichiometry of CaP can be identified reasonably well by APT.[45] Nevertheless, the amount of oxygen was lower and the amount of phosphorus was higher than predicted (for example, Ca/P = 1.41 and O/P = 3.33 were obtained for HAp, instead of the theoretical values 1.67 and 4.342, respectively[45]). Table 1 lists the bulk composition (at%), namely average for the whole sample for each element, as measured by LEAP tomography.

Comparing the Ca/P and O/Ca values for the bulk chemical composition with the theoretical values of different CaPs (see Table 3 in ref. 1), it is evident that there are not any good matches for the entire single phase. It could be argued that the Ca/P and O/Ca ratios alone are insufficient to determine unambiguously the phase contents. Yet, it can be stated that this region of the coating consists of a mixture of phases with a lower Ca/P ratio compared to HAp.

The presence of the precursor phase(s) discovered closest to the substrate is not surprising. As discussed, according to

Table 1 Bulk chemical composition (at%) determined by LEAP tomography

Element	at%
O	38.82 ± 0.13
H	29.27 ± 0.11
Ca	15.03 ± 0.04
P	11.79 ± 0.07
C	5.07 ± 0.04
N	0.01 ± 0.002
Ca/P	1.28 ± 0.01
O/Ca	2.58 ± 0.02

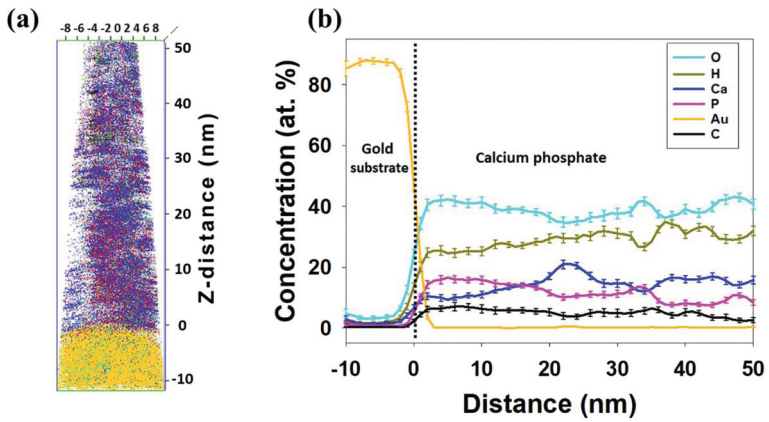

Fig. 1 (a) 3-D APT reconstruction based on 312 000 field-evaporated atoms from a nanotip. Calcium (blue), phosphorus (pink), oxygen (cyan), carbon (black), hydrogen (khaki), and gold (orange) are indicated. (b) 1-D concentration profiles of decomposed atoms along the *z*-axis of the nanotip, that is the longest axis. The colors of the symbols match the colors of the same type of atoms in part (a).

Ostwald's rule,[51] different phases have been suggested as precursors to HAp *in vivo*.[7,26–30,52–65] It is claimed that the structural relationships among these phases and the slow kinetics of HAp precipitation cause the formation of a precursor.[58]

Eliaz and Eliyahu suggested that the ED of HAp may occur *via* one of three routes: (1) a local pH increase that leads directly to precipitation in solution as a result of reaching the solubility limit; (2) acid–base reactions that lead to precipitation in solution when reaching the solubility product K_{sp}; and (3) electrochemical reactions.[5] Eliaz *et al.* further discussed the necessity for a high local pH value to deprotonate phosphoric acid to PO_4^{3-}, which is the most abundant species with a pH greater than 12.2, or even to HPO_4^{2-}, the predominant species within the pH range of 7.2 to 12.2.[5–8] Both PO_4^{3-} and HPO_4^{2-} are possible reactants in the chemical precipitation of HAp, OCP and other CaP phases; HPO_4^{2-} is the predominant species in the formation of CaP phases with low Ca/P atomic ratios, whereas PO_4^{3-} is the predominant species in the formation of CaP phases with high Ca/P atomic ratios. Eliaz *et al.* also noted that the very low solubility product of HAp and other CaP phases permits the precipitation of CaP even at relatively low concentrations of calcium and phosphate or hydrogen phosphate ions in the electrolyte.[8] It was also argued that the reason for no precursor phase being observed could be either due to its morphological and structural similarity to HAp, conversion over time to the more stable HAp, or the use of insensitive analytical techniques for the determination of the chemical composition of the coating at the

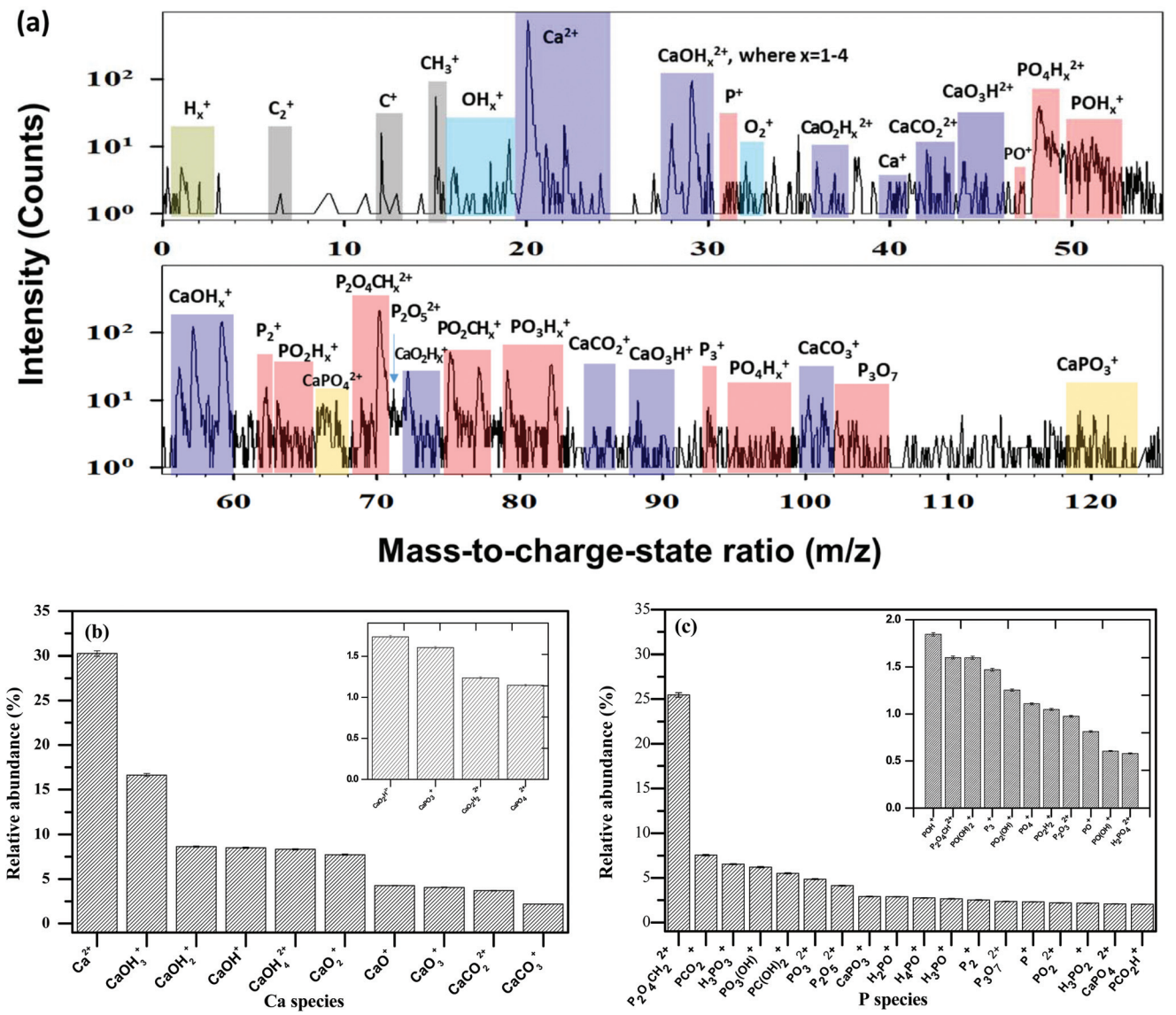

Fig. 2 (a) APT mass-to-charge spectra of ED CaP coated on a gold nanotip. Both the low and high mass regions are displayed (high and low figures, respectively). The peaks of the gold substrate were excluded from the mass spectrum for clarity. (b, c) The relative abundance of (b) Ca, and (c) P species in the ED CaP coating, calculated from the APT data. Note that the subscript *x* in the CaP hydrides in figure (a) is a number between 1 and 4.

heterophase interface with the substrate.[8] The present study does not suffer from this last limitation and proves that the precursor phase is present at the coating/substrate heterophase interface, and that it does not convert to HAp, at least not within the observed time scale. Further information on the full coating is presented below.

Obtaining unambiguous data is strongly dependent on controlling the different parameters of the LEAP tomograph; specifically the picosecond laser pulse energy. The greatest challenge with CaP ceramic-coated gold samples is the disparate evaporation fields of the two materials and their resulting evaporation rates, which makes data reconstruction difficult. The mass fragments of the surface species are seen in the mass spectra (Fig. 2(a)). These indicate the existence of Ca, O, P and H species (as well as C species) during field-evaporation. Small numbers of gold atoms are also present in the mass spectra of the coating at the interface with the gold substrate.

Based on the mass spectra, the relative abundances of different Ca and P species are calculated and presented in Fig. 2(b and c). The main species containing calcium in the mass spectra are presented in Table 2. The main species of phosphorus in the mass spectra are presented in Table 3. Note that the percentages in these tables are normalized per the total amount of species containing calcium or phosphorus, respectively.

From these data it is evident that the majority (~93.7%) of the phosphorus atoms evaporated from the specimen are part of molecular ions that contain oxygen. Most of the calcium atoms (~69.7%) evaporated from the specimen are also part of molecular ions that contain oxygen. This difference is not as large as that reported by Gordon *et al.*[45] who found that nearly all calcium (99.1%) was in the form of Ca^{2+}, the remaining 0.9% being $CaPO_3^+$ (in addition to a trace amount of CaO^+), compared to ~99.6% of the phosphorus atoms that were of oxygen-containing ions. Gordon *et al.*[45] argued that the P–O bond is stronger than the Ca–O bond under APT conditions, and that when phosphorus and calcium compete for oxygen, phosphorus wins in the vast majority of cases, probably due to the lesser covalent nature of the Ca–O bond and the reduced ability of calcium to engage in d-orbital-mediated, ligand-to-metal charge transfer. Herein, we find that only 2.8% of the calcium is part of phosphorus-containing molecular ions ($CaPO_3^+$ and $CaPO_4^{2+}$), while 66.9% is attached to oxygen-containing, phosphorus-free ions. This indicates that oxygen most likely bridges between Ca and P, as previously speculated.[45] In addition to a significantly smaller difference between the attachment of calcium and phosphorus ions to oxygen in the present research, compared to that reported by Gordon *et al.*, there is also a significant difference in the content of ions that are claimed to be a spectrometric fingerprint of single-crystal HAp, namely a series of ions of the general form $P_xO_y(OH)_z^+$, the major one being $PO_2(OH)^+$, which accounts for 63% of all detected hydroxyl groups. In the present study, $PO_3(OH)^+$, $PO(OH)_2^+$, $PO_2(OH)^+$ and $PO(OH)^+$ combined account for only ~9.7% of the total phosphorus-containing ions. These differences may be explained by the formation of a CaP phase that is not HAp in the present study, by the formation of a mixture of phases, or by the different synthesis routes (ED *versus* potassium sulfate flux).

Fig. 3(a) displays STEM Z-contrast of cross-sectional view of the CaP/Au heterophase interface. The STEM Z-contrast image reveals a CaP coating layer between the evaporated gold film and the Pt protective layer. The different contrast effects are due to the different atomic numbers of the elements and density variations in the coating. The dark dots in the electrochemically deposited CaP layer are associated with low-density regions (porous structure) inside the coating. The deposition was performed on an evaporated gold sample, which we recently performed for a different fundamental study.[18] A comparison between the electrodeposited APT nanotip and the evaporated gold sample observed *via* TEM can be made because they are similar, as they were coated using the same conditions in the same electrochemical cell. Fig. 3(a) demonstrates that the coating is porous. At a higher magnification, the pore diameter is observed to decrease as the coating evolves (see the inset in Fig. 3(a), in which some pores are marked by arrows). The pore diameter in the vicinity of the Au substrate is 15 ± 3 nm (utilizing ImageJ program). A diffraction

Table 2 The main species containing calcium in the mass spectra

Calcium species in the mass spectra	Percent
Ca^{2+}	30.3
$CaOH_3^+$	16.6
$CaOH_2^+$	8.6
$CaOH^+$	8.5
$CaOH_4^{2+}$	8.3
CaO_2^+	7.7
CaO^+	4.3
CaO_3^+	4.1
$CaCO_2^{2+}$	3.7
$CaCO_3^+$	2.2
CaO_2H^{2+}	1.7
$CaPO_3^+$	1.6
$CaO_2H_2^{2+}$	1.2
$CaPO_4^{2+}$	1.2

Table 3 The main species containing phosphorus in the mass spectra

Phosphorus species in the mass spectra	Percent	Phosphorus species in the mass spectra	Percent
$P_2O_4CH_2^{2+}$	25.4	PO_2^{2+}	2.2
PCO_2^+	7.6	$H_3PO_2^+$	2.2
$H_3PO_3^+$	6.5	$CaPO_4^{2+}$	2.1
$PO_3(OH)^+$or HPO_4^+	6.2	PCO_2H^+	2.0
$PC(OH)_2^+$	5.5	POH^+	1.8
PO_3^{2+}	4.8	$P_2O_4CH^{2+}$	1.6
$P_2O_5^{2+}$	4.1	$PO(OH)_2^+$ or $H_2PO_3^+$	1.6
$CaPO_3^+$	2.9	P_3^+	1.5
H_2PO^+	2.9	$PO_2(OH)^+$ or HPO_3^+	1.3
H_4PO^+	2.8	PO_4^+	1.1
H_3PO^+	2.7	$PO_2H_2^+$	1.0
P_2^+	2.5	$P_2O_3^{2+}$	1.0
$P_3O_7^{2+}$	2.4	PO^+	0.8
P^+	2.3	$PO(OH)^+$or HPO_2^+	0.6
		$H_2PO_4^{2+}$	0.6

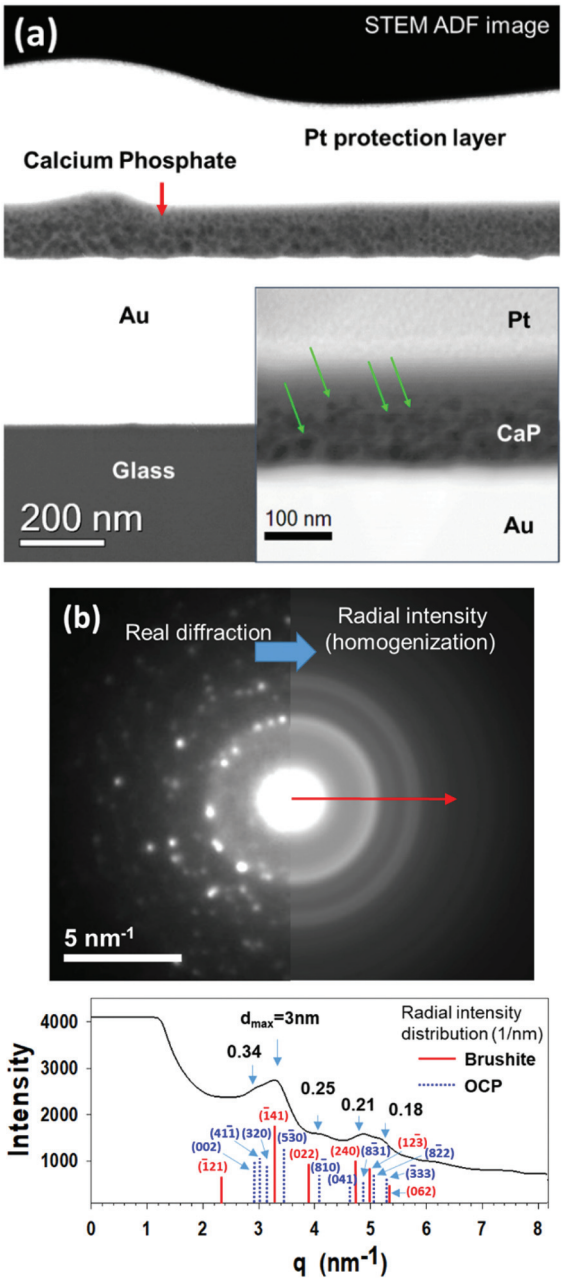

Fig. 3 (a) Cross-sectional TEM images revealing the different layers in the sample: glass substrate, evaporated gold, electrodeposited CaP, and Pt protection layer. The inset displays the porous structure of the CaP coating at a higher magnification. (b) Selected area diffraction pattern from the CaP coating adjacent to the Au substrate. The bottom part of (b) displays a radial intensity distribution, which reveals several *d*-spacing values related to different CaP phases.

pattern of the coating is displayed in Fig. 3(b), which is indicative of a mixture of phases in the deposited layer. The spot diffraction pattern represents two phases – brushite and OCP. Brushite (Ca/P = 1) has a monoclinic *Ia* (or, *I*2/*a*, if centrosymmetric) space group, with a = 5.812 ± 0.002 Å, b = 15.180 ± 0.003 Å, c = 6.239 ± 0.002 Å, and β = 116.42° ± 0.03°.[1,66] OCP (Ca/P = 1.33) has a triclinic $P\bar{1}$ space group, with a = 9.529 Å, b = 18.994 Å, c = 6.855 Å, α = 92.33°, β = 90.13°, γ = 79.93°.[1,60] Additionally, the diffuse background ring (halo) pattern indicates the presence of ACP in the coating. ACP is always considered to be metastable. Its chemical formula is $Ca_xH_y(PO_4)_z{\cdot}nH_2O$, where n = 3–4.5 and the water content is 15–20%. The composition of the precipitate depends on the composition and pH of the electrolyte solution; Ca/P = 1.2–2.2 has been reported.[1]

In addition to brushite, the reflections in the polycrystalline ring pattern indicate that at least one additional phase is present, but at a lower volume fraction. The radial intensity distribution of the selected area electron diffraction (SAED) pattern displayed in Fig. 3(b) reveals two distinct phases, with estimated *d*-spacings of 0.28 nm and 0.33 nm. Matching the CaP phases to the parameters obtained by TEM and SAED pattern analyses yields a mixture of ACP, DCPD and OCP phases. These TEM data, in conjunction with the APT data that yield a Ca/P value of 1.08 to 1.28, are clear evidence for the existence of transient precursor phases in the CaP coating, which have not yet been transformed into, or serve as a template for the growth of HAp. Thus, the correlative use of APT and TEM in this study provides an unprecedented sensitivity, which permits the unambiguous identification of the precursor phases that first grow on the gold substrate.

Before concluding, it is worthwhile noting that Münzenberg and Gebhardt observed the presence of both DCPD and OCP in the bone of young animals, based on X-ray diffraction (XRD) patterns.[67] A similar phase mixture is reported herein. The absence of HAp may be explained by the slow kinetics of the ED process, which was performed at 37 °C and pH = 7.4. Wang *et al.*[11] characterized the nanostructure of HAp ED at 85 °C and pH = 6.0 by means of scanning electron microscopy (SEM) and TEM. Two distinct layers were observed: (1) a dense 500 nm thick layer adjacent to the substrate, consisting of nano-sized (~50 nm) crystallites of polycrystalline HAp; and (2) a much thicker top layer consisting of single-crystal platelet HAp with varying sizes, preferentially grown perpendicular to the substrate surface. Herein, due to the lower bath temperature and different pH values, none of the phases grown adjacent to the substrate is HAp, and the thicker top-layer with a columnar HAp structure has not yet formed.

4. Conclusions

In summary, the interface of an electrodeposited CaP coating was studied in great detail on a well-defined gold substrate. APT in correlation with TEM discovered a mixture of phases, ACP, DCPD and OCP, and all could eventually serve as transient precursor phases to HAp. The layer containing these phases is tens of nanometers thick. TEM also revealed the porous nature of the coating, which changes in density during its growth. APT spectrometric analyses demonstrate that oxygen bridges calcium and phosphorus ions in the structure. This is the first study of electrodeposited CaP by means of APT, which demonstrates that the use of insensitive analytical

characterization techniques, and not very fast kinetics of phase transformation to HAp, is most likely the reason for missing these precursor phases in prior studies of electrodeposited CaP. The results of this study could have farther implications for *in vivo* studies of biomineralization, as well as in the synthesis of biomimetic CaP coatings.

Conflicts of interest

There are no conflicts to declare.

Acknowledgements

N. M. thanks the U.S.-Israel Binational Science Foundation (BSF) for awarding her a Prof. R. Rahamimoff travel grant, and the Tel-Aviv University Center for Nanoscience and Nanotechnology for awarding her a Tel-Aviv University/Northwestern University travel grant. The authors thank Mr Sumit Bhattacharya for technical assistance with the dual-beam FIB microscope at Northwestern University. We also thank Prof. Derk Joester and Ms Karen De Rocher for their assistance in the APT mass spectra analysis. APT was performed at the Northwestern University Center for Atom-Probe Tomography (NUCAPT). The local-electrode atom-probe tomograph at NUCAPT was acquired and upgraded with equipment grants from the MRI program of the National Science Foundation (grant number DMR-0420532) and the DURIP program of the Office of Naval Research (grant numbers N00014-0400798, N00014-0610539, N00014-0910781, N00014-1712870). NUCAPT is a Research Facility at the Materials Research Center of Northwestern University and received support through the National Science Foundation's MRSEC program (grant number NSF DMR-1720139) and from the Soft and Hybrid Nanotechnology Experimental (SHyNE) Resource (NSF ECCS-1542205). Additional instrumentation at NUCAPT was supported by the Initiative for Sustainability and Energy at Northwestern (ISEN).

References

1 N. Eliaz and N. Metoki, *Materials*, 2017, **10**, 334.
2 T. M. Sridhar, N. Eliaz, U. Kamachi Mudali and B. Raj, *Corros. Rev.*, 2002, **20**, 255–293.
3 N. Eliaz, T. M. Sridhar, U. Kamachi Mudali and B. Raj, *Surf. Eng.*, 2005, **21**, 238–242.
4 H. Wang, N. Eliaz, Z. Xiang, H.-P. Hsu, M. Spector and L. W. Hobbs, *Biomaterials*, 2006, **27**, 4192–4203.
5 N. Eliaz and M. Eliyahu, *J. Biomed. Mater. Res., Part A*, 2007, **80**, 621–634.
6 N. Eliaz and T. M. Sridhar, *Cryst. Growth Des.*, 2008, **8**, 3965–3977.
7 N. Eliaz, *Isr. J. Chem.*, 2008, **48**, 159–168.
8 N. Eliaz, W. Kopelovitch, L. Burstein, E. Kobayashi and T. Hanawa, *J. Biomed. Mater. Res., Part A*, 2009, **89**, 270–280.
9 D. Lakstein, W. Kopelovitch, Z. Barkay, M. Bahaa, D. Hendel and N. Eliaz, *Acta Biomater.*, 2009, **5**, 2258–2269.
10 N. Eliaz, S. Shmueli, I. Shur, D. Benayahu, D. Aronov and G. Rosenman, *Acta Biomater.*, 2009, **5**, 3178–3191.
11 H. Wang, N. Eliaz and L. W. Hobbs, *Mater. Lett.*, 2011, **65**, 2455–2457.
12 N. Eliaz, O. Ritman-Hertz, D. Aronov, E. Weinberg, Y. Shenhar, G. Rosenman, M. Weinreb and E. Ron, *J. Mater. Sci. Mater. Med.*, 2011, **22**, 1741–1752.
13 N. Metoki, L. Leifenberg-Kuznits, W. Kopelovich, L. Burstein, M. Gozin and N. Eliaz, *Mater. Lett.*, 2014, **119**, 24–27.
14 N. Metoki, L. Liu, E. Beilis, N. Eliaz and D. Mandler, *Langmuir*, 2014, **30**, 6791–6799.
15 H. Zanin, C. Rosa, N. Eliaz, P. May, F. Marciano and A. Lobo, *Nanoscale*, 2015, **7**, 10218–10232.
16 N. Metoki, D. Mandler and N. Eliaz, *Cryst. Growth Des.*, 2016, **16**, 2756–2764.
17 N. Metoki, C. M. R. Rosa, H. Zanin, F. R. Marciano, N. Eliaz and A. O. Lobo, *Surf. Coat. Technol.*, 2016, **297**, 51–57.
18 N. Metoki, K. Sadman, K. Shull, D. Mandler and N. Eliaz, *Electrochim. Acta*, 2016, **206**, 400–408.
19 R. Zhang, N. Metoki, O. Sharabani-Yosef, H. Zhu and N. Eliaz, *Adv. Funct. Mater.*, 2016, **26**, 7965–7974.
20 O. Geuli, N. Metoki, N. Eliaz and D. Mandler, *Adv. Funct. Mater.*, 2016, **26**, 8003–8010.
21 M. B. Thomas, N. Metoki, D. Mandler and N. Eliaz, *Electrochim. Acta*, 2016, **222**, 355–360.
22 M. B. Thomas, N. Metoki, O. Geuli, O. Sharabani-Yosef, T. Zada, M. Reches, D. Mandler and N. Eliaz, *ChemistrySelect*, 2017, **2**, 753–758.
23 O. Geuli, N. Metoki, T. Zada, M. Reches, N. Eliaz and D. Mandler, *J. Mater. Chem. B*, 2017, **5**, 7819–7830.
24 Z. Grubač, M. Metikoš-Huković and R. Babić, *Electrochim. Acta*, 2013, **109**, 694–700.
25 M. Metikoš-Huković, R. Babic, Z. Grubač, M. Petravić and R. Peter, *J. Electrochem. Soc.*, 2013, **160**, H674–H680.
26 M. D. Grynpas and S. Omelon, *Bone*, 2007, **41**, 162–164.
27 M. S. A. Johnsson and G. H. Nancollas, *Crit. Rev. Oral Biol. Med.*, 1992, **3**, 61–82.
28 R. Z. LeGeros, *Z. Kardiol.*, 2001, **90**(Suppl. 3), III116–III125.
29 W. E. Brown, J. P. Smith, J. R. Lehr and A. W. Frazier, *Nature*, 1962, **196**, 1050–1055.
30 P. Bodier-Houllé, P. Steuer, J. C. Voegel and F. J. G. Cuisinier, *Acta Crystallogr., Sect. D: Biol. Crystallogr.*, 1998, **54**, 1377–1381.
31 S. Shadanbaz and G. J. Dias, *Acta Biomater.*, 2012, **8**, 20–30.
32 D. N. Seidman, *Annu. Rev. Mater. Res.*, 2007, **37**, 127–158.
33 M. K. Miller and R. G. Forbes, *Mater. Charact.*, 2009, **60**, 461–469.
34 D. N. Seidman and K. Stiller, *MRS Bull.*, 2009, **34**, 717–721.
35 Y. Y. Tu, E. Y. Plotnikov and D. N. Seidman, *Microsc. Microanal.*, 2015, **21**, 480–490.
36 S. I. Baik, X. Yin and D. N. Seidman, *Scr. Mater.*, 2013, **68**, 909–912.

37 S. Mukherjee, U. Givan, S. Snez, A. Bergeron, S. Francoeur, M. de la Mata, J. Arbiol, T. Sekiguchi, K. M. Itoh, D. Isheim and D. N. Seidman, *Nano Lett.*, 2015, **15**, 3885–3893.
38 C. Monachon, D. C. Dunand and D. N. Seidman, *Small*, 2010, **6**, 1728–1731.
39 H. Takamizawa, Y. Shimizu, K. Inoue, T. Toyama, N. Okada, M. Okada, M. Kato, H. Uchida, F. Yano, A. Nishida, T. Mogami and Y. Nagai, *Appl. Phys. Lett.*, 2011, **99**, 133502.
40 H. Sepehri-Amin, W. F. Li, T. Ohkubo, T. Nishiuchi, S. Hirosawa and K. Hono, *Acta Mater.*, 2010, **58**, 1309–1316.
41 V. Vovk, G. Schmitz and R. Kirchheim, *Microelectron. Eng.*, 2003, **70**, 533–538.
42 T. Kinno, H. Akutsu, M. Tomita, S. Kawanaka, T. Sonehara, A. Hokazono, L. Renaud, I. Martin, R. Benbalagh, B. Sallé and S. Takeno, *Appl. Surf. Sci.*, 2012, **259**, 726–730.
43 Y. Zhang, J. Ai, A. C. Hiller and K. R. Hebert, *Langmuir*, 2012, **28**, 1673–1677.
44 S. Baik, A. Duhin, P. J. Phillips, R. F. Klie, E. Gileadi, D. N. Seidman and N. Eliaz, *Adv. Eng. Mater.*, 2016, **18**, 1133–1144.
45 L. M. Gordon, L. Tran and D. Joester, *ACS Nano*, 2012, **6**, 10667–10675.
46 L. M. Gordon and D. Joester, *Nature*, 2011, **469**, 194–198.
47 J. Karlsson, G. Sundell, M. Thuvander and M. Andersson, *Nano Lett.*, 2014, **14**, 4220–4223.
48 A. Stoffers, C. Oberdorfer and G. Schmitz, *Langmuir*, 2012, **28**, 56–59.
49 D. Palmer and M. Conley, *CrystalMaker for Windows Version 2.0.7*, CrystalMaker Software Ltd, 2008.
50 Y. Doi, Y. Moriwaki, T. Aoba, M. Okazaki, J. Takahashi and K. Joshin, *J. Dent. Res.*, 1982, **61**, 429–434.
51 W. Z. Ostwald, *Phys. Chem.*, 1897, **22**, 289–302, (in German).
52 L. Wang and G. H. Nancollas, *Met. Ions Life Sci.*, 2010, **4**, 413–456.
53 L. J. Brecevic and H. Furedi-Milhofer, *Calcif. Tissue Res.*, 1972, **10**, 82–90.
54 M. Nagano, T. Nakamura, T. Kokubo, M. Tanahashi and M. Ogawa, *Biomaterials*, 1996, **17**, 1771–1777.
55 A. L. Boskey, *J. Dent. Res.*, 1997, **76**, 1433–1436.
56 D. Tadic, F. Peters and M. Epple, *Biomaterials*, 2002, **23**, 2553–2559.
57 J. Christoffersen, M. R. Christoffersen, W. Kibalczyc and F. A. Andersen, *J. Cryst. Growth*, 1989, **94**, 767–777.
58 M. D. Francis and N. C. Webb, *Calcif. Tissue Res.*, 1970, **6**, 335–342.
59 O. Suzuki, S. Kamakura and T. Katagiri, *J. Biomed. Mater. Res., Part B*, 2006, **77**, 201–212.
60 W. E. Brown, N. Eidelman and B. Tomazic, *Adv. Dent. Res.*, 1987, **1**, 306–313.
61 K. Onuma and A. Ito, *Chem. Mater.*, 1998, **10**, 3346–3351.
62 J. Mahamid, B. Aichmayer, E. Shimoni, R. Ziblat, C. Li, S. Siegel, O. Paris, P. Fratzl, S. Weiner and L. Addadi, *Proc. Natl. Acad. Sci. U. S. A.*, 2010, **107**, 6316–6321.
63 C. Combes and C. Rey, *Acta Biomater.*, 2010, **6**, 3362–3378.
64 J. C. Elliott, *Structure and Chemistry of the Apatites and other Calcium Orthophosphates*, Elsevier, Amsterdam, The Netherlands, 1994.
65 B. Ben-Nissan, *Advances in Calcium Phosphate Biomaterials*, Springer, Dordrecht-Heidelberg-London-New York, 2014.
66 C. Beevers, *Acta Crystallogr.*, 1958, **11**, 273–277.
67 K. J. Münzenberg and M. Gebhardt, *Dtsch. Med. Wschr.*, 1969, **94**, 1325–1330.